Click Here for Full Article

Basin-scale soil moisture dynamics and the probabilistic characterization of carrier hydrologic flows: Slow, leaching-prone components of the hydrologic response

G. Botter,[1] A. Porporato,[2] I. Rodriguez-Iturbe,[3] and A. Rinaldo[1]

[1]   This paper aims at a first theoretical step toward the probabilistic modeling of nutrient contents in catchment-scale soil states. To this end, we wish to characterize probabilistically the slow, leaching-prone component of the hydrologic response, which chiefly determines the export of dissolved nutrients from soil, as a result of interactions between mobile/immobile phases along the pathways of runoff formation. The influence of temporal fluctuations of soil moisture on slow components of the catchment-scale runoff is thus investigated by means of a stochastic framework, where the intermittency of rainfall is modeled by a marked Poisson process with exponentially distributed intensities. The probability distribution of the relevant runoff components and its moment-generating function are derived by coupling a stochastic description of soil moisture dynamics with a suitably simplified flow model. New exact solutions are achieved in two different cases, namely, when (1) infiltration rates are assumed proportional to the incoming rainfall depths, i.e., when surface runoff is negligible, and (2) infiltration rates are upwardly bounded by episodical soil saturations (e.g., for shallow soils). In both cases, the derived probability density functions of slow components of runoff are well described by a Gamma distribution, whose shape is controlled by the ratio between the runoff frequency and the inverse of the mean residence time of subsurface flow. The framework developed allows one to link the probabilistic structure of slow components of runoff with simple (pluviometric, soil, vegetation, and geomorphologic) macroscopic parameters, with implications for the ecohydrology of fluvial systems and for drought prediction in ungauged basins. Comparisons with Monte Carlo simulations of a more detailed rainfall-runoff model to a real catchment located in northeastern Italy suggest the ability of the approach proposed to capture the main features of runoff probability distributions in heterogeneous catchments.

1. Introduction

[2]   The hydrologic runoff at the closure of a river basin is the byproduct of complex hydrometeorological and ecological processes. The pronounced temporal variability of runoff obviously reflects the random characters of key hydrologic fluxes, but also the heterogeneity of the transport dynamics in channeled and unchanneled regions of the basin. A proper analytical characterization of the statistical properties of the different components of runoff thus represents a challenging task because of the large number of stochastic processes involved, which require to be properly modeled at the scales of interest (i.e., the basin scale). This paper aims at a first theoretical step toward the probabilistic modeling of nutrient contents in hydrologic-scale soil states. Actually, our aim is to find reasonable analytical expressions for the stationary state of the probability distribution of soil nutrient concentrations. This is a natural extension of pioneering works [*Rodriguez-Iturbe et al.*, 1999; *Rodriguez-Iturbe and Porporato*, 2004] where the dynamics of water-controlled vegetation was tackled by studying the stationary probability distribution of soil moisture. To this end one needs to characterize, among other things, the slow, leaching-prone component of the hydrologic response (i.e., the base flow), which chiefly determines the export of dissolved nutrients from soil, as a result of interactions between mobile/immobile phases along the pathways of runoff formation.

[1]Dipartimento di Ingegneria Idraulica, Marittima e Geotecnica and International Center for Hydrology "Dino Tonini," Università di Padova, Padua, Italy.

[2]Department of Civil and Environmental Engineering, Duke University, Durham, North Carolina, USA.

[3]Department of Civil and Environmental Engineering, Princeton University, Princeton, New Jersey, USA.

[3] The analytical approach originated by *Rodriguez-Iturbe et al.* [1999] and further developed by *Laio et al.* [2001], *Porporato et al.* [2004], and *Rodriguez-Iturbe and Porporato* [2004] is aimed at the probabilistic modeling of the soil moisture dynamic at a point and provides an explicit linkage between temporal soil moisture fluctuations and underlying climatic and ecohydrologic processes. According to the above approach, the temporal dynamic of the soil water content is seen as the result of deterministic, state dependent loss processes (e.g., evapotranspiration, leakage) and stochastic (positive) increments driven by intermittent rainfall forcings.

[4] Several analytical and numerical studies [*Milly and Dunne*, 1993; *Porporato et al.*, 2004; *Botter et al.*, 2006] have shown that similar stochastic equations can also be employed to describe the average soil moisture content over entire hydrologic catchments. At the basin scale, in fact, the soil moisture loss function can be typically simplified and described by macroscopic effective parameters. Here, following *Porporato et al.* [2004], the analytical approach developed by *Rodriguez-Iturbe et al.* [1999] for modeling the water balance at a point is reinterpreted and applied to describe the temporal evolution of the average soil water content in heterogeneous catchments. The episodical exceedance of some critical level s_1 (comprised between the field capacity and complete saturation) is seen as the triggering mechanism for water release from soil toward the catchment outlet. The stochastic character of the rainfall volumes contributing to runoff is thus strictly related to the temporal fluctuations of soil moisture. It should be noted that the approach of linking basin-scale soil moisture content (or surface storage) to streamflow production is typical of some semidistributed hydrologic models [e.g., *Kavetsky et al.*, 2003]. Moreover, *Rodriguez-Iturbe et al.* [2006] recently extended the above quantitative general basis to both temporal and spatial intertwined dynamics.

[5] In this paper, a stochastic description of soil moisture dynamics and of the rainfall volumes contributing to runoff is coupled with a simplified transport scheme to provide an analytical characterization of the probability distribution function (pdf) of base flows in river basins. The main features of the base flow pdf are thus directly linked to macroscopic rainfall properties, to relevant soil-vegetation parameters, and to basic morphological features, with implications for the ecohydrology of fluvial systems, in particular for what concerns the analysis of drought frequency and low flows. It is worth emphasizing that the base flow pdfs derived in this paper are deduced on the basis of spatially averaged, catchment-scale properties. We therefore neglect effects related to the detailed description of the network morphology and of the spatial distribution of soil properties. Nevertheless, the effect of complex network structures and of heterogeneous soil, rainfall and vegetation properties on the statistical properties of the overall discharge can be actually included in the proposed framework. The above issues, however, would render the analytical treatment of the problem by far more complex and will be discussed elsewhere.

[6] The paper is organized as follows: Section 2 discusses the stochastic nature of the effective rainfall series due to the random character of the soil moisture dynamic in river basins. The probability distributions of the catchment-scale slow runoff components are then derived in section 3, where two different infiltration schemes are discussed. Section 4 presents the comparison of the analytical model with numerical results, derived from the Monte Carlo application of a numerical rainfall-runoff model to a real catchment located in northeastern Italy.

2. Soil Moisture Dynamics and the Production of Surface Runoff and Deep Percolation

[7] The soil moisture dynamics and the related runoff production mechanisms at the catchment scale are mostly controlled by the temporal variability of rainfall processes, which strongly affect the water balance in the hydrologically active topsoil layer. Following *Rodriguez-Iturbe et al.* [1999], the rainfall occurrence is here modeled as a zero-dimensional Poisson process of rate λ_P $[T^{-1}]$ (Figure 1a). The latter assumption postulates catchments sizes smaller than the correlation scale of rainfall events and timescales greater than the characteristic duration of single rainfall events (e.g., daily), so that the internal spatial and temporal structure of rainfall events can be neglected. Moreover, we model the dynamics of catchment-averaged soil moisture (and the ensuing runoff production mechanisms) as a state-dependent point process taking place in the topsoil layer, which is assumed to be labeled by constant, spatially averaged properties (e.g., depth, Z_r $[L]$, porosity, n (dimensionless), soil moisture, s (dimensionless)). Lateral flows in the upper soil layer are neglected, possibly preventing the extension of the approach described in this paper to the case of steep mountain basins, where lateral flows play a decisive role in soil saturation dynamics during intense rainfall events. Daily rainfall depths, h $[L]$, are assumed to be exponentially distributed with parameter γ'_P (Figure 1a) and the dominant runoff production mechanism is supposed to be Dunnian (as typical in flat temperate regions). Furthermore, we neglect ecosystem dynamics, thus focusing on average, constant hydroecological parameters (i.e., representative of a whole season). Under the above assumptions, the procedure employed by *Rodriguez-Iturbe and Porporato* [2004] to derive the steady state probability distribution of soil moisture at a point can be interpreted and applied to heterogeneous catchments, where spatially averaged soil moisture pdfs can be described by macroscopic (rainfall, soil and vegetation) parameters [*Porporato et al.*, 2004; *Botter et al.*, 2006]. Under the above assumptions, the mass balance within the topsoil layer of a catchment can be written in terms of the spatially averaged (relative) soil moisture, $s(t)$, as

$$\frac{ds(t)}{dt} = -\rho[s(t)] + \xi_t. \tag{1}$$

The last term of equation (1), ξ_t, represents stochastic instantaneous inputs due to infiltration from rainfall. The latter is modeled as a marked Poisson process of rate λ_P and normalized depths, $h/(nZ_r)$, extracted from an exponential distribution of parameter $\gamma_P = \gamma'_P nZ_r$

$$\xi_t(\lambda_P; \gamma_P) = \sum_{i;t_i < t} \frac{h_i}{nZ_r} \delta(t - t_i), \tag{2}$$
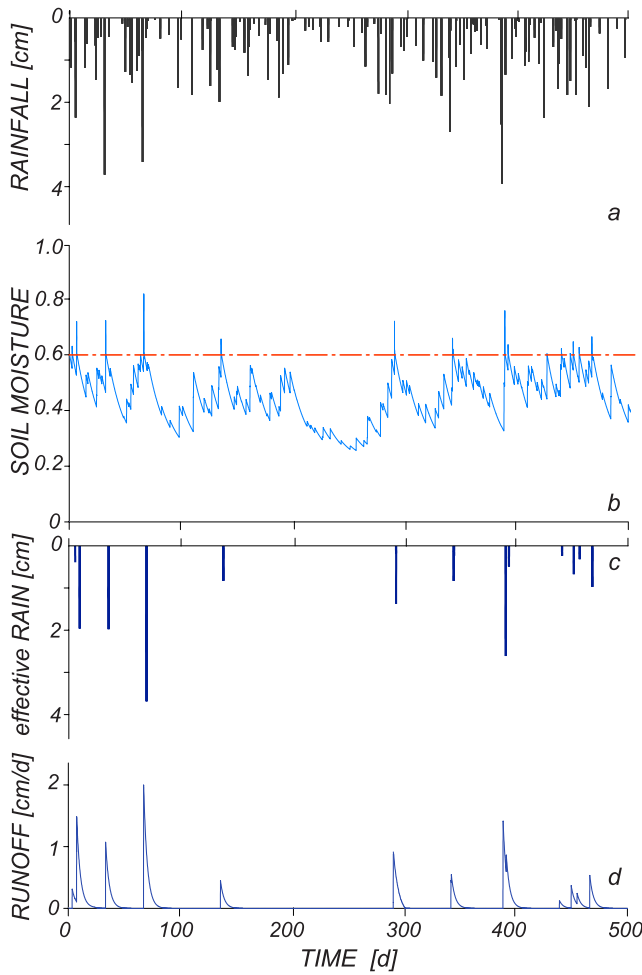
Figure 1. Schematic representation of the soil moisture and runoff models: (a) Temporal evolution of the overall rainfall depths (synthetic data). The interarrivals and the rainfall depths are exponentially distributed with a frequency $\lambda_P = 0.3$ d^{-1} and with the following values of the parameter controlling the (normalized) intensities: $\gamma_P = 16.6$, respectively. (b) Temporal evolution of the (catchment averaged) relative soil moisture, $s(t)$, which is commanded by the intermittent rainfall forcings shown in Figure 1a and by the deterministic decay due to evapotranspiration process, according to equation (1). The dash-dotted line represents the threshold s_1, whose up crossing determines the triggering of runoff events. (c) Temporal sequence of effective rainfall, driven by the exceedence of the threshold s_1 for the soil moisture $s(t)$. (d) Temporal evolution of the overall, specific (i.e., for unit area) discharge. The soil, vegetation, and transport parameters employed for this simulations are $n = 0.55$, $Z_r = 30$ cm, $s_w = 0.18$, $s_1 = 0.6$, $ET_{max} = 0.35$ cm/d, and $k = 0.6$ d^{-1}.

where δ is the Dirac delta function. Thus the interarrival times between subsequent rainfall events are distributed according to an exponential distribution of parameter λ_P. The term $\rho[s(t)]$ in equation (1) is the (normalized) catchment-scale soil loss function. For the sake of simplicity we focus here on the case of linear loss functions, which have been proved to be a reasonable approximation of actual evapotranspiration fluxes, particulary when considering large spatial scales [e.g., *Wetzel and Chang*, 1987; *Porporato et al.*, 2004]

$$\rho(s) = \frac{(s - s_w)}{(s_1 - s_w)} \frac{ET_{max}}{nZ_r} \qquad (s \leq s_1), \qquad (3)$$

where s_1 is a critical soil moisture level, typically larger than field capacity [e.g., *Porporato et al.*, 2004]. For soil moisture levels below s_1 rainfall is assumed to instantaneously infiltrate (at the daily timescale), while above s_1 rainfall is assumed to be instantaneously lost as deep percolation and/or surface runoff [*Porporato et al.*, 2004]. Note that soil moisture levels above s_1 can be reached only due to the instantaneous duration of the rainfall pulses. According to equation (3), evapotranspiration is assumed to vanish below the wilting point, s_w, and linearly increasing above s_w up to a maximum rate, ET_{max} [L][T^{-1}].

[8] The master equation for the evolution of the spatially averaged basin-scale relative soil moisture pdf can be obtained as described by *Rodriguez-Iturbe et al.* [1999]. The corresponding steady state solution in the case of linear losses can be expressed by a truncated gamma distribution

$$p(s) = c(s - s_w)^{\frac{\lambda_P}{\eta} - 1} \exp(-\gamma_P s), \qquad (4)$$

where c is the normalization constant [see *Porporato et al.*, 2004] and η is the normalized maximum evapotranspiration rate, i.e., $\eta = E_{max}/[nZ_r(s_1 - s_w)]$.

[9] The production of surface runoff and/or deep percolation in the considered catchment is schematically illustrated in Figure 1b. When the spatially averaged, relative soil moisture $s(t)$ exceeds the threshold s_1, the water volumes exceeding s_1 are instantaneously lost from the upper soil layer (Figure 1c). They constitute the effective rainfall for the catchment, i.e., the fraction of rainfall that propagates within the hillslopes and eventually reaches the outlet through the channel network. A key point that needs to be addressed in order to describe the probabilistic structure of streamflow at the daily timescale is thus the statistical characterization of the occurrences of surface runoff and/or deep percolation, which embeds the random character of the rainfall input, as well as the interaction between ecological and hydrologic processes.

[10] According to our simplified scheme, the distribution of the occurrence of surface runoff and/or deep percolation is determined by the soil moisture crossing of the threshold $s = s_1$. A complete description of the distribution of the crossing times L, $p_L(L)$, [T^{-1}], presents serious analytical difficulties [*Rodriguez-Iturbe and Porporato*, 2004]. However, the mean crossing time can be quite easily expressed in terms of the soil moisture pdf as [*Porporato et al.*, 2001; *Rodriguez-Iturbe and Porporato*, 2004]

$$\langle L \rangle = \frac{1}{\rho(s_1)p(s_1)}. \qquad (5)$$

The numerical pdfs of runoff interarrivals $p_L(L)$ (suitably normalized with respect to the mean interarrival $\langle L \rangle$) obtained from Monte Carlo simulations of the soil moisture model described by equations (1)–(3) are shown in Figure 2,
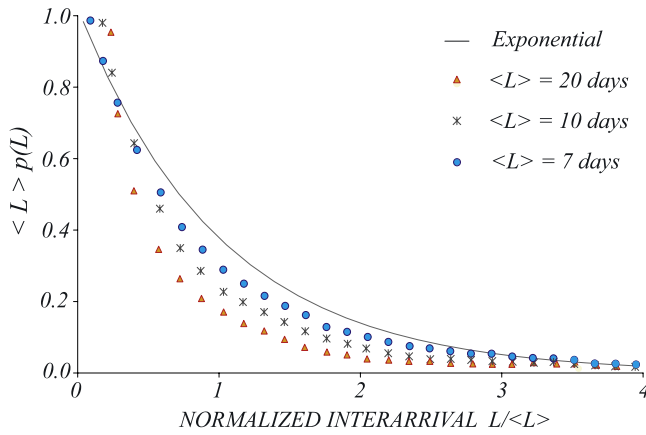
Figure 2. Results from the numerical Monte Carlo simulation of the soil moisture model: probability density function of the runoff interarrivals L, $p_L(L)$ (normalized with the average runoff interarrival $\langle L \rangle$), for different values of the mean runoff interarrival $\langle L \rangle$: 7 days (circles), 10 days (crosses), and 20 days (triangles). The solid line represents the exponential distribution. The parameters employed for the simulations presented are $s_w = 0.18$, $s_1 = 0.6$, $E_{max} = 0.3$ cm/d, $\lambda_P = 0.3$ d^{-1}, $n = 0.55$, and $Z_r = 30$ cm. The average rainfall depths are 0.8 cm (triangles), 1.2 cm (crosses), and 3 cm (circles).

where we explore runoff frequencies ranging from 0.05 d^{-1} (circles) to 0.14 d^{-1} (triangles). The graph reported in Figure 2 suggests that the actual distribution of the interarrivals is relatively well approximated by an exponential distribution (solid line) as the runoff frequency increases. We thus assume that the exponential distribution is a reasonable approximation of the runoff interarrival distribution, particularly when the ratio between the average runoff interarrival, $\langle L \rangle$, and the characteristic time of the loss process (e.g., $(s_1 - s_w)nZ_r/ET_{max}$) is smaller than 0.1, and we rely on numerical simulations to assess the influence of the above approximation on the ensuing runoff pdf (see section 3.3). A similar simplification was adopted also by *Laio* [2006], even though in a different context.

[11] On the basis of the above considerations, we can model the temporal evolution of the effective rainfall depths, I [L], as a new marked Poisson process, whose frequency λ is linked to the underlying probability distribution of soil moisture according to the following relationship

$$\lambda = \rho(s_1)p(s_1). \tag{6}$$

From now on we shall refer to λ as the runoff frequency, regardless of the fate (surface runoff and/or subsurface flow) of the rainfall volumes exceeding the threshold s_1 (see below). Thus the rate of stochastic runoff and/or deep infiltration events, commanded by the temporal evolution of the soil moisture in the topsoil layer, is described as

$$\xi'_t(\lambda; \gamma'_P) = \sum_{j:t_j<t} I_j \delta(t - t_j), \tag{7}$$

where the effective rainfall depths, I, are assumed to be exponentially distributed with parameter γ'_P (see also Figure 3 and the discussion therein) and the intervals between subsequent events, $L = t_{j+1} - t_j$, are sampled from an exponential distribution with parameter λ, whose value is crucially dependent on rainfall properties and on soil and vegetation parameters.

[12] It is also interesting to observe that the soil moisture dynamics that transform (through the threshold s_1) the total rainfall into effective rainfall, from a mathematical standpoint, act as a special form of censoring process on the overall rainfall series. The underlying soil moisture dynamic, in fact, changes the mean frequency of the original rainfall process (from λ_P to λ), but it does not alter the distribution of the depths, which remains exponential with mean $1/\gamma'_P$. From an analytical point of view, this means that soil moisture acts on rainfall variability as an effective interception. The formalism developed by *Rodriguez-Iturbe et al.* [1999] to describe the fraction of rainfall not intercepted by plant canopy can thus be transferred in this context to describe the production of runoff and/or deep infiltration from the total rainfall.

3. Probability Distribution of Slow Components of the Hydrologic Response

[13] According to the runoff production model described above, surface runoff is assumed to be triggered by the complete soil saturation (i.e., $s = 1$). It constitutes the fast component of the hydrologic response and is thus deemed responsible of producing discharge at timescales shorter than 1 day. In order to achieve a relatively simple mathematical treatment of the problem, however, we shall neglect
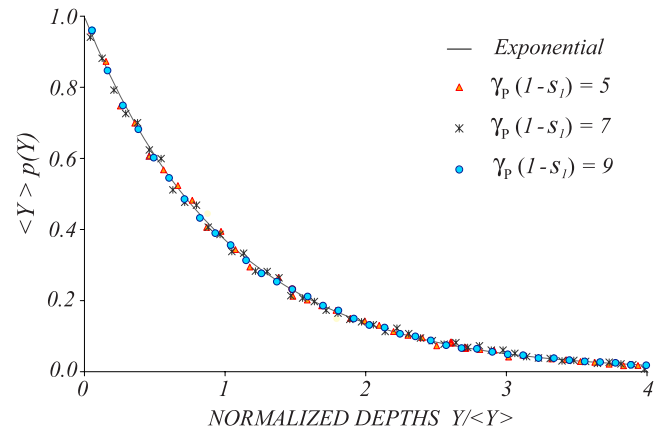
Figure 3. Results from the numerical Monte Carlo simulation of the soil moisture model: Probability density function of the effective rainfall intensities Y, $p_Y(Y)$, suitably normalized with the average rainfall intensity $\langle Y \rangle$ for different values of the parameter $r = \gamma_P (1 - s_1)$ (see text): $r = 5$ (triangles), $r = 7$ (crosses), and $r = 9$ (circles). The corresponding mean runoff interarrivals $\langle L \rangle$ are 10 days (circles), 15 days (crosses), and 20 days (triangles). The solid line represents the exponential distribution. The average rainfall depths are 0.8 cm (triangles), 1.0 cm (crosses), and 1.2 cm (circles). The other soil, vegetation, and rainfall parameters are those employed in Figure 2.

the fraction of effective rainfall propagating as surface runoff, thus focussing on deep infiltration dynamics and its role in streamflow formation. Therefore we derive probability distributions for the slow component of the hydrologic response and we explicitly neglect the surface contribution originated during intense storm events. For this reason the terms "runoff" or "discharge" in what follows are employed to indicate the streamflow contribution originated from subsurface processes (i.e., the base flow). Furthermore, we note that slow components of the hydrologic response can be identified with daily discharges in relatively small basins (i.e., when the characteristic timescale for surface processes is much shorter than 1 day): under the above circumstances, in fact, the integration over a time period larger than the characteristic time of surface processes usually beclouds the contribution of the fast component of the hydrologic response to the overall (catchment-scale) runoff pdf.

[14] Deep percolation and subsurface runoff, instead, are assumed to be triggered when the soil moisture s exceeds the threshold s_1. In particular, the deep percolation depths, Y, are assumed to be equal to the pertinent effective rainfall depth, I, if the effective rainfall is lower than $(1 - s_1)\, nZ_r$ and equal to $(1 - s_1)\, nZ_r$ when $I > (1 - s_1)\, nZ_r$ (e.g., when the soil is saturated). The rainfall depths contributing to deep percolation (i.e., leakage), Y, are thus upwardly bounded by the threshold $nZ_R\,(1 - s_1)$, which represents the leakage volume in correspondence of soil saturation.

[15] The water pulses deeply infiltrating into soil, Y, are then transported as subsurface flow and they are eventually released toward the stream network. The search for coherent transport models capable of reproducing the water dynamics in soil and predicting catchment-scale hydrologic responses has inspired a large part of the hydrologic literature in the last decades. This is due to the fact that the water transport in river basins is a complex process, characterized by pronounced heterogeneities operating at different spatial and temporal scales. Furthermore, a complete description of all relevant soil water processes can hardly be made through field observations.

[16] It should be noted that while the approach presented here is not a rainfall-runoff model (as none of the key assumptions would hold), it is reasonable to relate it to the context of rainfall-runoff models as deterministic or stochastic descriptors of the various components of the hydrologic response, thus including those sought after herein. As we show for comparison in section 3.1, the slow component that interests us could be obtained by suitably filtering the output of complete models. In that context, deterministic models are rather often applied in the form of spatially distributed approaches, which include three dimensional, grid element based models coupling surface and subsurface flow [e.g., *Bathurst et al.*, 1995; *Bathurst and Cooley*, 1996], land-atmosphere interactions [e.g., *Wood et al.*, 1997] and topography-based models [e.g., *Beven and Kirkby*, 1979; *Sivapalan et al.*, 1990; *Beven et al.*, 1995; *Beven*, 2001]. Catchment-scale hydrologic responses of river basins have been also described by the use of lumped models, for which a certain degree of conceptualization of the physical processes involved is inevitably introduced. In this context, the pioneering paper of *Rodriguez-Iturbe and Valdes* [1979] showed the equivalence between the instan-

taneous unit hydrograph and the probability distribution of the residence times τ (i.e., the traveltime of a water particle within the basin seen as the control volume for the transport process). It turned out to be of particularly significance because the stochastic formulation of transport by traveltime distributions proved a general and profound theoretical framework for basin-scale processes of various nature pertaining both surface and subsurface hydrology [e.g., *Dagan*, 1989; *Rodriguez-Iturbe and Rinaldo*, 1997].

[17] In view of the main objective of the paper (i.e., the analytical derivation of the pdf for the slow component of the hydrologic response), a residence time approach is here employed for modeling subsurface transport processes at the catchment scale. The postulated absence of pronounced topographic effects, in fact, prevent from the use of more detailed models exploiting topographic properties. Furthermore, the framework based on the residence time distribution allows one to embed the effect of heterogeneities of dynamical and geomorphological properties in a single curve (i.e., the probability distribution of the residence time, $f(\tau)$). In the literature, different types of residence time distributions have been used to model the hydrologic response of a river basin [e.g., *Gupta et al.*, 1980; *Rinaldo et al.*, 1991, 1995]. In the present paper we adopt a simplified scheme, where the effects of the network structure (and of the spatial organization of the drainage pathways) on the ensuing basin-scale hydrologic response are neglected. This is consistent with the spatial and temporal scales considered in this study, that allow to model the rainfall as a sequence of uniform and instantaneous (i.e., daily) inputs. The whole catchment is simply modeled as a linear reservoir, where the outflowing flux is assumed proportional to the water storage. This is tantamount to assume that the catchment-scale subsurface flow is characterized by an exponential residence time distribution (i.e., $f(\tau) = k \exp(-k\tau)$, if k is the inverse of the mean residence time). Even though theoretical and experimental reservations have been noted [*McGuire et al.*, 2005; *Troch et al.*, 2004], the exponential distribution has been widely employed in the literature [e.g., *Boyd*, 1978; *Rinaldo et al.*, 2006a], because it allows one to reproduce the slow release of water from soil and it requires a single calibration parameter. Furthermore, extensive validations against field data have proved the robustness of the linear assumption in modeling subsurface flows at large spatial scales in many cases of practical interest [e.g., *Rinaldo et al.*, 2006b].

[18] The overall catchment-scale runoff Q (in the sense specified above) is thus linked to the temporal evolution of the deep infiltration depths, $Y(t)$, according to the following relationship (see also Figure 1)

$$Q(t) = A \int_0^t Y(t - \tau) f(\tau) d\tau, \qquad (8)$$

where A is the basin surface, and $f(\tau) = k \exp(-k\tau)$. A Langevin equation for runoff can be obtained deriving both sides of equation (8) with respect to t,

$$\frac{dQ(t)}{dt} = -kQ(t) + kA\xi_t'', \qquad (9)$$

where the first term on the right-hand side represents the deterministic (exponential) decay of the discharge due to the slow release of water from soil and the last term on the right-hand side represents the stochastic rate due to inputs by deep percolation

$$\xi_t''(\lambda) = \sum_{j:t_j<t} Y_j \delta(t - t_j). \tag{10}$$

Note that the intervals between subsequent deep percolation events, $t_{j+1} - t_j$, are exponentially distributed with parameter λ (exactly as the total effective rainfall). Accordingly, the master equation for the probability distribution of the discharge $p(Q, t)$ can be written as

$$\frac{\partial p(Q,t)}{\partial t} = \frac{\partial[kQp(Q,t)]}{\partial Q} - \lambda p(Q,t) + \lambda \int_0^Q p(Q - z, t)\, b(z)dz, \tag{11}$$

where $b(Q)$ indicates the distribution of runoff increments, $\Delta Q = kAY$. The local temporal variation of the runoff probability, $p(Q, t)$, can thus be expressed as the sum of three independent terms: the probability gain due to the deterministic decay caused by slow release of water from hillslopes; the loss of probability due to jumps forcing the system to leave the discharge level Q; and the increment of probability due to positive jumps from lower discharge levels. The solution of equation (11) is related to the specification of the pdf of the runoff increments, $b(Q)$, as a function of the effective rainfall, as discussed in the following paragraphs.

3.1. Unbounded Runoff Jump Distribution (Negligible Surface Runoff)

[19] In many cases, when the soil is relatively thick and permeable, deep infiltration and subsurface runoff are much more important than surface runoff in determining the probabilistic structure of base flows. Let r be the ratio between the soil storage capacity above the threshold s_1 and the average daily rainfall

$$r = \gamma_P(1 - s_1). \tag{12}$$

When $r \gg 1$, we may neglect the upper bound in the distribution of the water volumes infiltrating during rainfall events represented by the soil saturation (i.e., $s = 1$). Under the above assumption, the deep percolation depths Y have the same exponential distribution of the effective rainfall depths. This is shown numerically by Figure 3, where we plot the deep percolation depths pdf, $p_Y(Y)$, derived by the Monte Carlo simulation of the soil moisture model, for values of r ranging from 5 (circles) to 9 (triangles). The numerically obtained leakage probability distributions shown in Figure 3 are suitably normalized with respect to the mean depth $\langle Y \rangle$ and refer to mean runoff frequencies λ ranging from 0.05 d^{-1} (circles) to 0.1 d^{-1} (triangles). In all the cases explored the distribution of the effective rainfall depths closely fits the expected exponential distribution (solid line). As a

consequence, the following exponential distribution applies to the discharge jumps

$$b(Q) = \gamma_Q \exp\left(-\gamma_Q Q\right), \tag{13}$$

where the inverse of the mean discharge increment due to incoming effective rainfall events is

$$\gamma_Q = \gamma_P/(n\,k\,A\,Z_r). \tag{14}$$

Under such circumstances, the master equation for the runoff probability distribution (equation (11)) reads

$$\frac{\partial p(Q,t)}{\partial t} = \frac{\partial[k\,Q\,p(Q,t)]}{\partial Q} - \lambda p(Q,t)$$
$$+ \lambda\gamma_Q \int_0^Q p(Q - z, t) \exp\left(-\gamma_Q z\right) dz, \tag{15}$$

whose steady state solution can be shown to be a Gamma distribution

$$p(Q, t \to \infty) = c^* Q^{\left(\frac{\lambda}{k} - 1\right)} \exp\left(-\gamma_Q Q\right), \tag{16}$$

where $c^* = \gamma_Q^{\lambda/k}/\Gamma(\frac{\lambda}{k})$ is the normalization constant. The mean and the variance of the runoff pdf can be easily expressed in term of the parameters λ, k and γ_Q as

$$\langle Q \rangle = \frac{\lambda}{k\gamma_Q}$$
$$\langle Q^2 \rangle - \langle Q \rangle^2 = \frac{\lambda}{k\gamma_Q^2}. \tag{17}$$

Note that the probability distribution of base flows given by equation (16) can be considered to account also for the presence of a channelized network connecting the groundwater system to the catchment outlet. In fact, after neglecting hydrodynamic dispersion (which is known to bear a negligible effect on the main features of the hydrologic response at the basin scale [see, e.g., *Robinson et al.*, 1995; *Botter and Rinaldo*, 2003]), the runoff propagation within a channel reach mainly produces a kinematic delay between the output signal (i.e., the runoff) and the forcing noise (i.e., the deep percolation), without affecting the probabilistic structure of the steady state probability distribution of runoff. According to equation (16), the probability distribution of base flows is related to the undergoing soil and vegetation properties (through the parameter λ) and to the key rainfall properties (through both the parameters γ_Q and λ), but it also depends on important geomorphic factors such as the mean residence time of the groundwater flow ($1/k$) and the size of the basin (A). The shape of the runoff pdf is chiefly controlled by the ratio between the runoff frequency, λ, and the inverse of the mean residence time in subsurface, k. When $\lambda/k > 1$ ("wet conditions") the pdf of the runoff is bell-shaped with $p(Q = 0) = 0$ (i.e., very low discharges are characterized by zero probability, see Figure 4), while for $\lambda/k < 1$ ('dry conditions') $p(Q)$ goes to infinity for $Q \to 0$, and it monotonically decreases for $Q > 0$, approaching zero as $Q \to \infty$. The critical condition $\lambda = k$, which determines the shift between the 'wet regime' and the 'dry regime' can be expressed in term of basic rainfall, soil and vegetation properties by the use of equation (6). Among
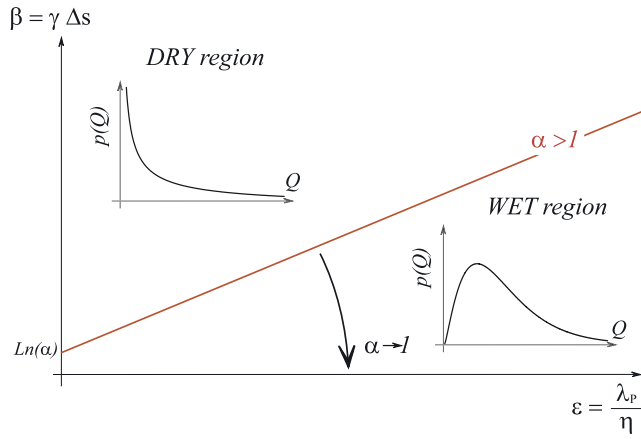
Figure 4. Graphical (qualitative) representation of the dependence of daily runoff pdf on the dimensionless parameters α, β, and ϵ provided by equations (18)–(20). The solid line qualitatively represents the condition $\lambda = k$ (which determines the transition from the "dry" to the "wet" region) in the (ϵ, β) plane in the case $\alpha > 1$. As $\alpha \to 1^+$, the transition line approaches the x axis, and the wet region progressively vanishes. As a consequence, for $\alpha < 1$ we only observe monotone pdf belonging to the dry regime, regardless of the values of the parameters β and ϵ.

all the possible choices, we shall express the transition condition in term of three dimensionless groups:

$$\epsilon = \frac{\lambda_P}{\eta} \tag{18}$$

$$\beta = \gamma_P \Delta s \tag{19}$$

$$\alpha = \frac{\lambda_P}{k}, \tag{20}$$

where $\Delta s = s_1 - s_w$. The dimensionless parameters ϵ, β, α defined by equations (18)–(20) express the ratio between the characteristic time of evapotranspiration processes and the mean interarrival between rainfall events, the ratio between the soil storage volume and the mean daily rainfall volume, and the ratio between the rainfall rate and the rate of water release from soil, respectively. By using equation (6), and expressing both $p(s)$ and $\rho(s)$ in terms of ϵ, β and α, the transition between the "dry" and "wet" regimes (i.e., the inequalities $\lambda < k$ and $\lambda > k$) can be expressed as follows:

$$\alpha \frac{\exp(-\beta)\beta^\epsilon}{\epsilon[\Gamma(\epsilon) - \Gamma(\epsilon, \beta)]} < 1 \quad \Rightarrow \quad \text{dry regime}$$

$$\alpha \frac{\exp(-\beta)\beta^\epsilon}{\epsilon[\Gamma(\epsilon) - \Gamma(\epsilon, \beta)]} > 1 \quad \Rightarrow \quad \text{wet regime} \tag{21}$$

The transition between the above regimes is shown in Figure 4, which graphically represents the dependence of the runoff pdf on the dimensionless parameters α, β and ϵ. The solid line depicts the condition $\lambda = k$ in the (ϵ, β) plane, in the case $\alpha > 1$. As $\alpha \to 1^+$, however, the transition line approaches the x axis, and the wet region progressively vanishes. The condition $\alpha < 1$ is thus

sufficient (even though not necessary) for the existence of a monotonous "dry" runoff pdf. We observe that runoff pdfs of the "wet" type are unlikely to be observed in nature, owing to the fact that in many circumstances the average interarrival between rainfall events is larger than the mean residence time within the catchment (i.e., α is typically smaller than one).

[20] The key role exerted by the ratio λ/k in determining the shape of the runoff pdf is also shown by Figure 5, where we compare the analytical solution given by equation (16)
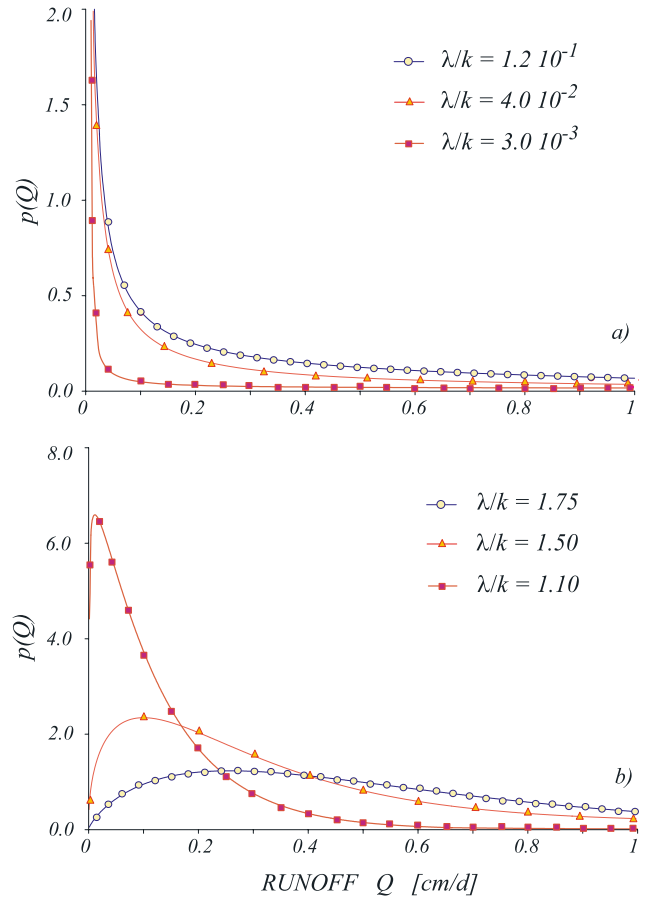
Figure 5. Numerical validation of the analytical runoff pdf (equation (16)) and sensitivity analysis in the case of unbounded infiltration. (a) Analytical probability distribution of daily runoff (solid line) in the case of dry conditions ($\lambda_P = 0.2$ d^{-1}, $E_{max} = 0.35$ cm/d and $k = 0.5$ d^{-1}) for different values of the average daily rainfall ($\gamma_P = 30$, 16, 10). The ensuing ratios λ/k (i.e., the product between the runoff frequency, λ, and the mean residence time in subsurface, $1/k$) are 0.003, 0.04, and 0.12, respectively. The simulated values of the runoff pdf resulting from the Monte Carlo application of the runoff model provided by equation (9) are reported as circles ($\lambda/k = 0.12$), triangles ($\lambda/k = 0.04$), and squares ($\lambda/k = 0.003$). (b) Same as Figure 5a but for wet conditions ($\lambda_P = 0.45$ d^{-1}, $E_{max} = 0.15$ cm/d and $k = 0.2$ d^{-1}). The resulting values of the ratio λ/k are in this case greater than 1: $\lambda/k = 1.1$ (circles), $\lambda/k = 1.5$ (triangles), and $\lambda/k = 1.75$ (squares). Common parameters to all the simulations shown are $s_w = 0.18$, $s_1 = 0.6$, $n = 0.55$, and $Z_r = 30$ cm. Note that the resulting values of r (see text) are 4 (circles), 7 (triangles), and 12 (squares).

with the Monte Carlo simulations of the runoff model for different values of the rainfall and vegetation parameters in the case of unbounded runoff increments. Figure 5a refers to the case of "dry" runoff pdfs, corresponding to average runoff interarrivals greater than the mean catchment residence time. As the average rainfall depth increases (in the examples reported in Figure 5a from 0.6 cm (squares) to 1.65 cm (circles)) the ensuing average runoff frequency decreases, leading to decreasing values of the ratio λ/k (from 0.003 to 0.12 d^{-1}). Figure 5a shows how the distance between the runoff pdf and the origin of the axis tends to decrease as the frequency of runoff events, λ, decreases. Furthermore, according to equations (17) the first moments of the distribution (e.g., the mean and the variance) are linearly increasing with λ, whereas the probability of low discharges is decreasing with the runoff frequency. Figure 5b shows the behavior of the runoff pdf in the "wet" regime, which is related to average runoff interarrivals (in this case ranging from 4.5 days (squares) to 2.5 days (circles)) smaller than the mean catchment residence time $1/k$ (here about 5 days). Figure 5b also shows that the peak of the runoff pdf decreases with λ whereas the mode of the distribution increases. Note that all the simulations reported in Figure 5 refer to ratios between the soil storage capacity and the mean rainfall rate, r, larger than 4, therefore allowing the use of the simplified runoff jump pdf provided by equation (13).

3.2. Bounded Runoff Jump Distribution

[21] In this section we derive the probability distribution of base flows in the case when surficial runoff cannot be neglected, i.e. when the soil storage capacity is comparable with the average daily rainfall. If $r \leq 1$, the distribution of infiltrating volumes is significantly affected by the existence of the upper bound corresponding to the soil saturation (i.e., $s = 1$). Owing to the fact that the water volumes exceeding the threshold s_1 are assumed to be instantaneously released from the topsoil layer toward deeper soil layers, the percolation depths, Y, follow a truncated exponential distribution with the same parameter characterizing the distribution of the effective rainfall. Accordingly, the probability distribution of the runoff jumps, $b(Q)$, is given by

$$
b(Q) = \gamma_Q \exp\left(-\gamma_Q Q\right) H\left[\overline{Q} - Q\right]
$$
$$
+ \delta\left(Q - \overline{Q}\right) \int_{\overline{Q}}^{\infty} \gamma_Q \exp\left(-\gamma_Q Q\right) dQ, \quad (22)
$$

where $H[\cdot]$ is the Heaviside step function, $\delta(\cdot)$ is the Dirac-δ function and γ_Q is defined by equation (14). $\overline{Q}$ is the maximum available runoff increment due to incoming rainfall events (i.e., the runoff increment resulting from complete soil saturation)

$$
\overline{Q} = (1 - s_1) nkAZ_r = \frac{r}{\gamma_Q}. \quad (23)
$$

The corresponding master equation for the runoff probability distribution reads

$$
\frac{\partial p(Q,t)}{\partial t} = \frac{\partial[k\, Q\, p(Q,t)]}{\partial Q} - \lambda p(Q,t) + \lambda \gamma_Q \int_0^Q p(Q-z,t)
$$
$$
\cdot \exp\left(-\gamma_Q z\right) H\left[\overline{Q} - z\right] dz + \lambda p(Q - \overline{Q}, t)
$$
$$
\cdot \exp\left(-\gamma_Q \overline{Q}\right) H\left[Q - \overline{Q}\right], \quad (24)
$$

where the last term on the right-hand side represents the gain of probability due to rainfall events determining complete soil saturation. Equation (24) can be transformed in the Laplace domain ($Q \rightarrow u$), leading to the following first-order partial differential equation:

$$
\frac{1}{ku} \frac{\partial \widehat{p}(u,t)}{\partial t} = \frac{\partial \widehat{p}(u,t)}{\partial u} + \frac{\lambda}{k} \left\{ \frac{1 - \exp\left[-\overline{Q}\left(\gamma_Q + u\right)\right]}{\gamma_Q + u} \right\} \widehat{p}(u,t),
$$
$$
(25)
$$

where $\widehat{p}(u, t)$ is the Laplace transform of the runoff pdf $p(Q, t)$

$$
\widehat{p}(u,t) = \int_0^{\infty} \exp(-uQ) p(Q,t) dQ. \quad (26)
$$

The steady state solution of equation (25), $\widehat{p}(u)$, which represents the moment generating function of the runoff pdf, can be written as

$$
\widehat{p}(u) = \widetilde{c}\left(u + \gamma_Q\right)^{-\frac{\lambda}{k}} \exp\left\{ \frac{\lambda}{k} Ei\left[-\overline{Q}\left(\gamma_Q + u\right)\right] \right\}, \quad (27)
$$

where $Ei[\cdot]$ is the exponential-integral function and

$$
\widetilde{c} = \frac{\gamma_Q^{\frac{\lambda}{k}}}{\exp\left[\lambda Ei\left(-\overline{Q}\gamma_Q\right)/k\right]} \quad (28)
$$

is the normalization constant. According to equation (27), the runoff pdf can be expressed as the convolution between a Gamma distribution (which derives from the antitransformation of the polynomial part of the moment generating function (27)) and a nonanalytical function (the inverse transform of the exponential function appearing on the right-hand side of equation (27), whose effects on the ensuing runoff pdf decrease as $\overline{Q}$ increases). As expected, for $\overline{Q} \rightarrow \infty$ (i.e., when the surface runoff is negligible), equation (27) yields

$$
\widehat{p}(u) = \gamma_Q^{\frac{\lambda}{k}}\left(u + \gamma_Q\right)^{-\frac{\lambda}{k}}, \quad (29)
$$

whose inversion leads to the runoff pdf derived in section 3.1 (equation (16)).

[22] When the distribution of the runoff jumps, $b(Q)$, is bounded, the probability distribution of runoff cannot be specified in a closed form, owing to the fact that equation (27) cannot be inverted analytically. However, thanks to the properties of the moment generating functions, i.e.,

$$
\langle Q^n \rangle = \int Q^n p(Q) dQ = (-1)^n \frac{d^n \widehat{p}(u)}{du^n}\bigg|_{u=0}, \quad (30)
$$

suitable analytical expressions can be derived for the moments of the runoff pdf. From equations (27) and (23), the following expressions are obtained for the average runoff $\langle Q \rangle$ and for the corresponding variance, var(Q):

$$
\langle Q \rangle = \frac{\lambda}{k\gamma_Q}\left[1 - e^{-r}\right]
$$

$$
\text{var}(Q) = \langle Q^2 \rangle - \langle Q \rangle^2 = \frac{\lambda}{k\gamma_Q^2}\left[1 - (1 + r)e^{-r}\right]. \quad (31)
$$

The ratio between the first two moments of the runoff pdf in the case of bounded infiltration and the corresponding
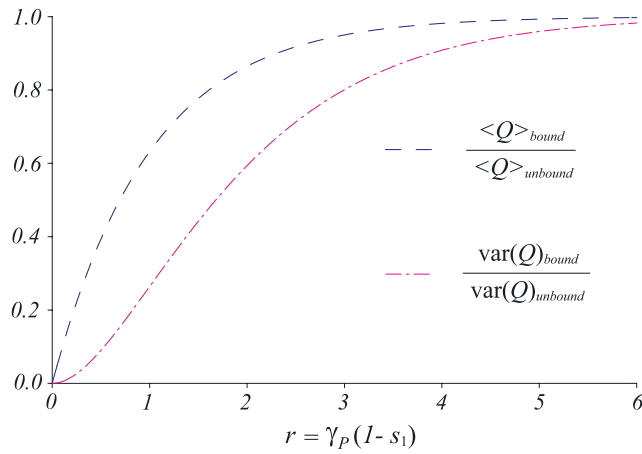
Figure 6. Effects of the upper bound in the runoff jump distribution, $b(Q)$, on the moments of the runoff probability distribution. The graph reports the ratio between the first two moments of the runoff pdf in the case of bounded infiltration (equations (31)) and the corresponding moments in the case of unbounded infiltration (equations (17)).
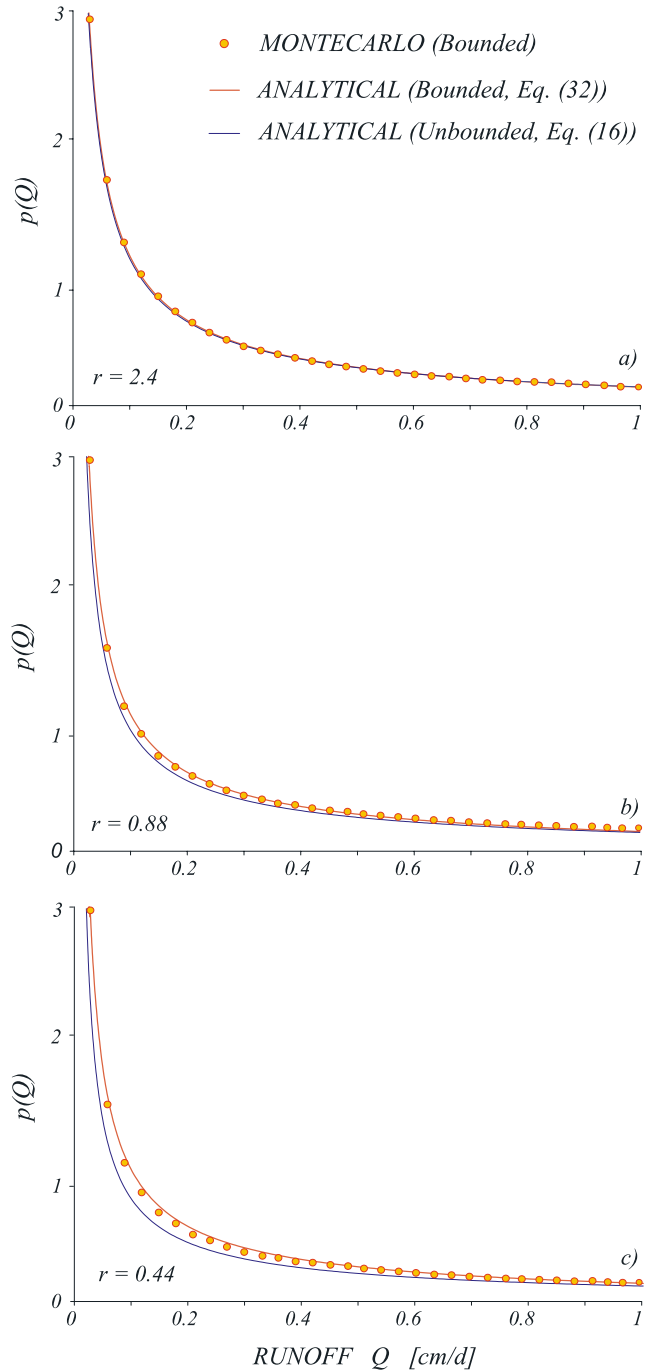
moments in the case of unbounded infiltration (equation (17)) are reported in Figure 6 as a function of r. Because of the fact that the terms in square brackets in equations (30) are smaller than unity, the first two moments of the runoff probability distribution in the case of shallow soils are always smaller than the corresponding moments in the case of unbounded runoff jumps (Figure 6). The upper bound of the runoff jumps therefore leads to an overall runoff distribution which is characterized by a shorter tail with respect to the case of unbounded infiltration. As expected, for $r \to \infty$ the factors appearing within square brackets on the right-hand side of equation (31) approach 1 (Figure 6), and the expressions derived in the case of unbounded infiltration (equation (17)) are straightforwardly recovered. Figure 6 also suggests that the effect of the upper bound in the runoff increments on the runoff probability distribution is more pronounced for the higher-order moments.

[23] The effect of the finite water storage capacity of the soil on the base flows probability distribution can be further investigated by the use of numerical Monte Carlo simulations. Figure 7 shows a comparison between the numerical runoff pdf in the case of bounded runoff jumps (circles) and the corresponding analytical runoff pdf derived in the case of unbounded infiltration (equation (16), dark solid line) for the case $\lambda < k$. The ratio between the soil storage capacity and the average daily rainfall depth, r, ranges from 2.4 (Figure 7a) to 0.44 (Figure 7c). Also shown (light solid line) is the approximated analytical Gamma distribution obtained rescaling the runoff distribution corresponding to the case of unbounded infiltration (equation (16)) so as to produce the same average base flow obtained for bounded infiltration

$$p(Q) = \frac{\gamma_Q'^{\lambda/k}}{\Gamma(\lambda/k)} Q^{\left(\frac{\lambda}{k}-1\right)} \exp\left(-\gamma_Q' Q\right), \qquad (32)$$

with

$$\gamma_Q' = \frac{\gamma_Q}{1 - e^{-r}}. \qquad (33)$$

Figure 7. Effect of the finite soil storage capacity on the daily runoff probability distribution (case $\lambda < k$, when the runoff frequency is smaller than the inverse of the mean residence time in subsurface): comparison of the numerical runoff pdf in the case of a bounded runoff jump pdf (circles) with the corresponding analytical pdf derived for unbounded infiltration (equation (16), dark solid line) and a rescaled Gamma distribution with the same average runoff $\langle Q \rangle$ obtained in the case of bounded infiltration (equation (32), light solid line). In all the simulations we assumed $n = 0.28$ (porosity) and $Z_r = 13$ cm (soil depth). The average rainfall intensities are (a) 0.6 cm, (b) 1.65 cm, and (c) 3.3 cm, leading to the values of r indicated. All the other parameters are the same as used in Figure 4.
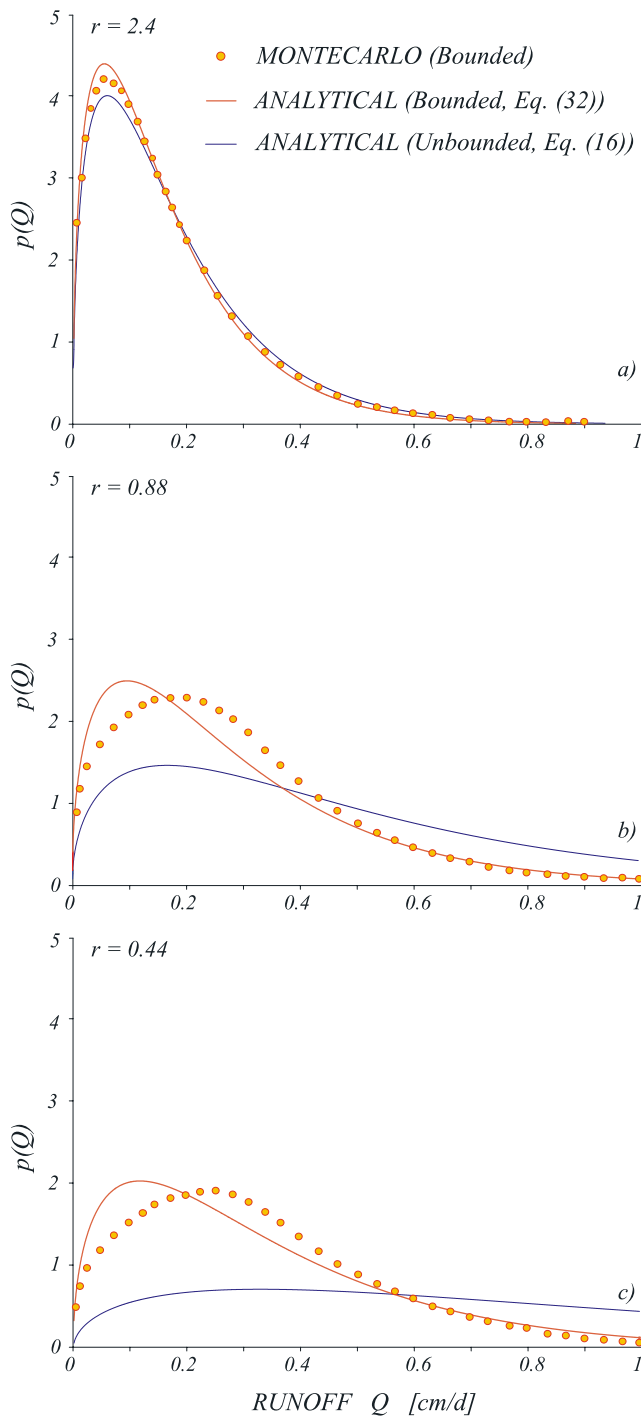
Figure 8. Effect of the finite soil storage capacity on daily runoff probability distribution (case $\lambda > k$, when the runoff frequency is larger than the inverse of the mean residence time in subsurface): comparison of the numerical runoff pdf corresponding to the case of a bounded runoff jump pdf (circles) with the corresponding analytical pdf derived in the case of unbounded infiltration (equation (16), dark solid line) and a rescaled Gamma distribution with the same average runoff obtained in the case of bounded infiltration (equation (32), light solid line). In all the simulations reported we assumed $n = 0.28$ and $Z_r = 13$ cm. The average rainfall intensities are (a) 0.6 cm, (b) 1.65 cm, and (c) 3.3 cm, leading to the values of r indicated. All the other parameters are the same as employed in Figure 5.

Figure 7 clearly shows that the effect of the upper bound of the runoff jump distribution on the runoff probability distribution is indeed small, in the dry regime, even for low values of r (Figure 7c). The above effect becomes completely negligible when $r > 1$ (Figure 7a). We note also that the approximated analytical Gamma distribution provided by equation (32) is a satisfactory approximation of the actual runoff pdf in all the cases explored.

[24] Figure 8 illustrates the same comparison shown in Figure 7 but for the case $\lambda > k$ (wet regime). We observe that in the 'wet' regime the effect due to the upper bound of the runoff jump distribution on the runoff probability distribution is more pronounced than in the dry regime. This is possibly due to the increase of runoff frequency, which emphasizes the differences in the distribution of runoff jumps. In such cases, significant differences related to the bound of the runoff jump pdf appear in the runoff distribution even when $r > 1$ (Figure 8a). Nevertheless, the rescaled Gamma distribution (equation (32)) is able to provide a reasonable approximation of the numerically obtained runoff distribution for all the runoff frequencies investigated. The approximate analytical solution, however, allows a proper description of the behavior of the actual runoff pdf only for relatively high values of the discharge, whereas a bias appears at low flows when $r \leq 1$ (Figures 8b and 8c). We also observe that the capability of the approximate solution (32) of capturing the main features of the runoff pdf decreases, in the case of bounded runoff jumps pdf, as the runoff frequency increases.

3.3. Leakage Interarrivals and Runoff Probability Distributions

[25] In the derivation of the analytical runoff pdfs, as well as in all the numerical simulations shown in sections 3.1 and 3.2, we assumed an exponential distribution of the leakage interarrivals, i.e., $p_L(L) \sim \exp(-L/\langle L \rangle)$. However, the actual runoff interarrival distribution (as it derives from the application of the soil moisture model, equation (1)), can be reasonably approximated by an exponential distribution only for large runoff frequencies (e.g., $\lambda \geq 0.15$ d^{-1}). When the occurrence of leakage events, as controlled by the soil moisture dynamic in the active soil layer, is a (relatively) rare circumstance, the actual runoff interarrival distribution leads to higher probabilities of the smallest interarrival times with respect to the exponential distribution (Figure 2). To asses the impact of the nonexponential behavior of the runoff interarrivals pdf, we compare the analytical runoff probability distribution derived in sections 3.1 and 3.2 with the numerical pdfs derived from the coupled Monte Carlo simulation of the soil moisture and runoff models (equations (1) and (9)). We focus on the case of relatively thick soils ($n = 0.55$ and $Z_r = 30$ cm) and "dry case" runoff pdfs ($\lambda_P = 0.3$ d^{-1}, $k = 0.5$ d^{-1}), because of the fact that the above circumstances ensure the lowest runoff frequencies. Figure 9a refers to an average runoff interarrival of 10 days and shows the comparison between the analytical runoff pdf (obtained assuming an exponential leakage interarrival distribution; solid lines) and the numerical results derived from the Monte Carlo application of the soil moisture and runoff models (where the leakage interarrivals are nonexponentially distributed, according to the soil moisture dynamic (circles)). We analyze both the cases of bounded (open circles) and
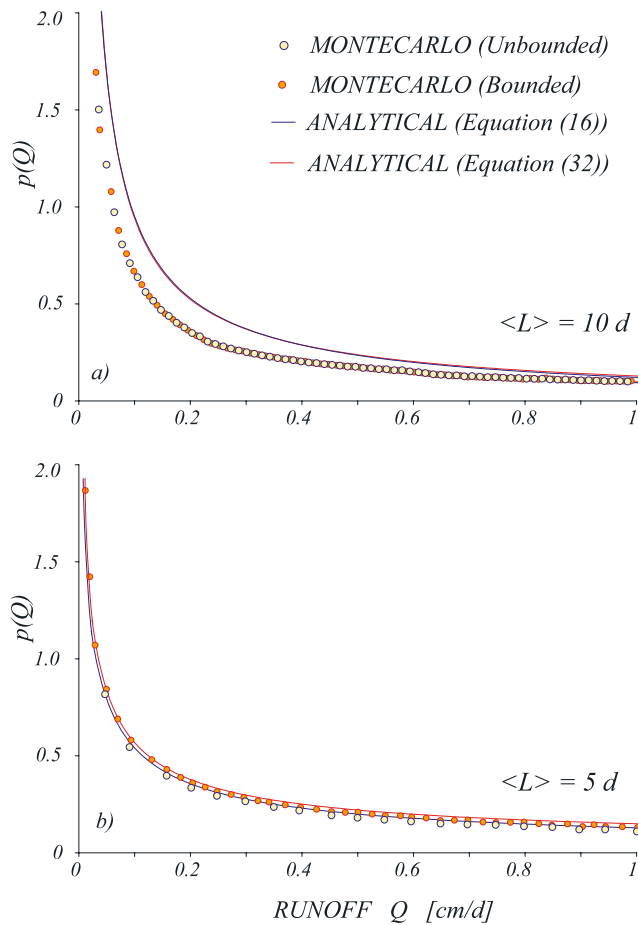
Figure 9. Complete numerical simulations of the soil moisture and runoff models in the case of unbounded runoff jump pdf (the porosity, n, is 0.55 and the active soil depth, Z_r, is 30 cm) in the case $\lambda < k$ (the rainfall frequency λ_P is 0.3 d^{-1}, whereas the transport parameter, k, is 0.5 d^{-1}). (a) Comparison between the analytical runoff pdf (solid lines lines) and the numerical results derived from the Monte Carlo application of the soil moisture and runoff models (circles). Both the case of bounded (open circles) and unbounded (shaded circles) infiltration are explored and compared to the pertinent analytical runoff probability distributions (equations (32) and (16), respectively). The average rainfall depth is 1.2 cm/d, leading to an average runoff interarrival of 10 days. (b) Same as Figure 9a but with an average rainfall depth of 3 cm/d, which leads to an average runoff interarrival of 5 days. Common parameters to both the simulations are s_w = 0.18, s_1 = 0.6, and E_{max} = 0.3 cm/d.

unbounded (shaded circles) infiltration. No significant differences due to the finite soil storage capacity emerge, owing to the fact that in this case $r \gg 1$. Figure 9a clearly shows how the higher probabilities characterizing the smallest interarrival times in the numerical leakage interarrival distribution produce a long-tailed runoff pdf, where the highest runoff values are characterized by larger occurrence probabilities with respect to the analytical runoff pdf derived in the case of exponential interarrivals. A similar effect could be obtained in the analytical runoff probability distributions

(equations (16) or (32)) by increasing the average daily rainfall (i.e., by decreasing the parameter γ_Q); see Figure 7. The effect of the nonexponential behavior of the leakage interarrivals could thus be included in the analytical model by suitably rescaling the leakage depths. Figure 9b (which refers to an average runoff interarrival of 5 days), instead, shows that when the average runoff frequency is relatively high, the analytical model based on the assumption of exponentially distributed interarrivals of runoff events is capable of predicting the numerical runoff probability distribution almost exactly. Note also that in such circumstances a small difference appears between the cases of bounded and unbounded infiltration, owing to the smaller value of the ratio, r, between the soil storage capacity and the average daily rainfall.

[26] We thus conclude that the analytical model given by equations (16) and (32), based on the assumption of exponential runoff interarrivals, provides a reasonable approximation of the runoff probability distribution in many cases of practical interest.

4. Comparison With a Detailed Geomorphic Model of the Hydrologic Response

[27] In order to test the robustness of the analytical approach developed in this paper, the derived probability distributions of base flows are compared in this section with numerical results obtained from the Monte Carlo application of a continuous, geomorphically based rainfall-runoff model to the Dese catchment closed at Villa Volpi (northeastern Italy). The Dese catchment closed at Villa Volpi is a 53 km^2 flat basin belonging to the drainage basin of the Venice Lagoon, where extensive hydrologic studies have been recently carried out [e.g., *Rinaldo et al.*, 2005; *Botter et al.*, 2006; *Rinaldo et al.*, 2006a, 2006b]. Runoff measurements in the Dese catchments are available (in continuous) at hurly time steps since 1999. Thus measured runoff time series does not allow a proper evaluation of the statistical properties of the discharges, owing to the limited extension of the sample. Moreover, discharge measurements are only available in tidal sections located downstream the closure section of Villa Volpi considered in this application. The above problem has been overstepped in the numerical studies cited above by means of the application of finite elements schemes capable of describing unsteady flows in open channels (for a detailed discussion, see *Rinaldo et al.* [2006b]). For the above reasons we shall rely on the comparison with numerical simulations rather than using observed runoff data sets.

[28] The detailed (numerical) continuous model of the hydrologic response employed is based on the synthetic generation of rainfall and climate series able to reproduce the statistical properties of the observed series. This allows to simulate the soil moisture dynamics and the ensuing runoff fluctuations in response to prescribed (e.g., observed) climate conditions. The stochastic generation of hourly rainfall series in the Dese catchment is obtained through the application of a (seasonally variable) cluster-based rainfall model of the Bartlett-Lewis type [see, e.g., *Rodriguez-Iturbe et al.*, 1987, 1988; *Botter et al.*, 2006]. Owing to the limited extent of the catchment at hand with respect to the characteristic spatial scale of rainfall events, we employ spatially uniform rainfall rates throughout the basin. It should

be noted, however, that the resulting net rainfall shows a certain spatial variability because of the heterogeneity of the hydraulic soil properties.

[29] The synthetic generation of daily climatic series (maximum and minimum temperature, maximum and minimum relative humidity, wind speed) has been achieved by the use of a stochastic multivariate $(AR(1))$ model which preserves the observed correlations between climatic variables [*Botter et al.*, 2006]. Possible fluctuations into the correlations among climatic variables due to the occurrence of rainfall events are also taken into account. The seasonal variability of daily climatic data is properly considered by considering each month separately.

[30] On the basis of the underlying network structure, suitably identified via topography and remote images [*Rinaldo et al.*, 2006b], the Dese catchment is subdivided into 17 subbasins, whose characteristic size is of the order of a few square kilometers. From the synthetically generated climate and rainfall series, a continuously updated description of the soil moisture dynamics within each subbasin is then achieved by the use of the Green-Ampt model for shallow soils [e.g., *Dingman*, 1994]. The Green-Ampt approach may account both for Dunnian and Hortonian runoff production mechanisms. In the case at hand, however, owing to the relatively weak average intensity of the incoming rainfall, the production of surface runoff is chiefly related to Dunnian processes, thus allowing the comparison with the analytical model developed in this paper. The Penman-Monteith equation integrated by the FAO approach is employed to compute evapotranspiration fluxes on the basis of (relatively) few micrometeorological, soil and vegetation parameters, whose spatial distribution has been determined via remotely sensed images. Accordingly with experimental evidences deriving from field data, the soil thickness and the porosity have been assumed uniform throughout the catchment and they have been suitably calibrated on the basis of continuous discharge measurements [*Rinaldo et al.*, 2006b]. In a similar manner, other relevant vegetation properties were calibrated for a single (predetermined) reference crop, while the vegetation parameters for all the other crops involved have been properly derived from the corresponding parameters obtained for the reference crop. Further details on the numerical water balance model employed are given by *Rinaldo et al.* [2006b]. Even though in the numerical model the mathematical computation of the water losses is somewhat more refined than that used in the derivation of the analytical runoff pdfs of section 3, the physical processes considered for estimating evapotranspiration and leakage losses in both the approaches are very similar. In particular, *Botter et al.* [2006] showed that the catchment-scale water losses resulting from the numerical, Monte Carlo model described above can be properly expressed in terms of the spatially averaged relative soil moisture, $s(t)$, through large-scale (i.e., effective) soil and vegetation parameters.

[31] As a result of the application of the rainfall, climate and water balance models, both the temporal evolution of the soil water content within each subbasin and the spatial distribution of the rainfall volumes contributing to runoff are achieved. The transport processes determining the propagation of the effective rainfall within each subbasin are then modeled following the geomorphological theory of the hydrologic response. Accordingly, the catchment is

thought of as a nested structure of units (i.e., hillslopes and channels), where the spatial distribution of runoff paths defines the characters of the traveltime distribution at the outlet of the basin. The units where paths originate (i.e., the subbasins of the catchment) are labeled by an area A_i whose size (e.g. $\sqrt{A_i}$) has been chosen to reasonably reproduce the observed drainage density. The overall catchment-scale travel time distribution, $f(t)$, is thus obtained by averaging individual path residence time distributions, which are in turn expressed by suitable convolutions of the traveltime distributions within the channels, $f_{c_i}(t)$, and the hillslopes, $f_{A_i}(t)$ [see *Rinaldo et al.*, 2006b]. Flow discharges are finally obtained by routing the net rainfall pulses provided by the water balance model.
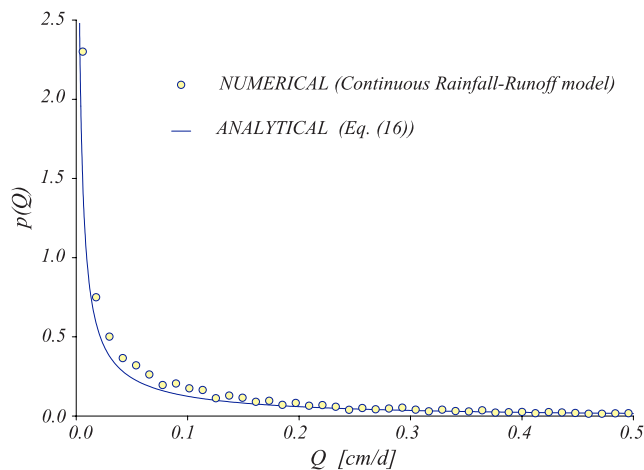
[32] The continuous, numerical rainfall-runoff model is run at time steps of a few minutes for 250 years, during which the meteorologic forcing is represented by the synthetic series derived through the rainfall and climate generators. The temporal evolution of the soil water content within each subcatchment and the spatial/temporal dynamics of effective rainfall are achieved by means of the water balance model. Finally, the application of the transport model allows to derive the streamflow at the outlet of each subcatchment and the runoff at the closure of the whole basin. The probability distribution of daily runoff can be thus easily estimated for each season by the use of standard techniques of sample analysis. In what follows we will refer to the runoff pdf for the spring season (from March to May).

[33] The aggregated parameters for the analytical model are derived from the Monte Carlo numerical model as follows: the corresponding average rainfall frequency, λ_P, and the normalized average daily rainfall, $1/\gamma_P$, of the Poissonian rainfall model are deduced on the basis of the synthetic rainfall series (during the springtime). It can be shown, in fact, that the statistical properties of the rainfall series derived through the application of the Barlett-Lewis model described above, once aggregated at daily time steps, do not differ much from that of a marked Poisson process (at list in the case at hand). In particular, both the distribution of the daily depths and that of the interarrivals between two subsequent wet days are nearly exponential. The same property is also exhibited by the rainfall time series recorded in a gauge station located nearby the considered test catchment.

[34] The soil thickness, Z_r, and the porosity, n, (which have been considered as spatially uniform in the Monte Carlo simulations) are derived by calibration of the numerical rainfall/runoff model during gauged runoff events. The mean residence time within the subsurface, $1/k$, is instead derived as a weighted average of the subsurface mean residence time within the different subbasins. In the numerical model, the mean residence time within the different subcatchments has been assumed to depend on the extent of the subbasins [see *Rinaldo et al.*, 2006b], thus allowing the calibration of a single parameter, i.e., the mean residence time in a reference subcatchment.

[35] The macroscopic, large-scale soil and vegetation parameters characteristic of the spring season (s_w, s_1, and E_{max}) are instead derived by interpolating the numerical relationship between the catchment-scale water losses, ρ, and the spatially averaged relative soil moisture, s, resulting from the Monte Carlo simulation, with an analytical func-

Figure 10. Comparison between the spring runoff pdf derived from the Monte Carlo application of the continuous geomorphically based rainfall-runoff models coupled with a stochastic rainfall generator (circles) and the corresponding analytical daily runoff probability distribution (equation (16)) in the Dese catchment. The parameters used in the the analytical model are congruent with the parameters employed in the numerical Monte Carlo rainfall-runoff model. The complete set of soil, vegetation, and transport parameters used by the continuous numerical rainfall-runoff model are given by *Rinaldo et al.* [2006b] and *Botter et al.* [2006]. The corresponding parameters used in the analytical model are $n = 0.55$ (porosity), $Z_r = 30$ cm (soil depth), $s_w = 0.18$ (wilting point), $s_1 = 0.6$ (deep percolation threshold), $E_{max} = 0.25$ cm/d (maximum evapotranspiration), $k = 0.6$ d^{-1} (inverse of the mean residence time in subsurface), $\lambda_P = 0.33$ d^{-1} (rainfall frequency), and $\gamma_P = 18.3$ (parameter controlling the distribution of the rainfall intesities).

tion of the type expressed by equation (3). The resulting daily runoff pdf is then calculated on the basis of equation (16); note that in this case the upper bound in the runoff jump distribution is negligible. The comparison between the numerical runoff pdf derived from the Monte Carlo application of the climate, water balance and rainfall-runoff models (circles) and the corresponding analytical runoff probability distribution (equation (16)) is shown in Figure 10. It is worth mentioning that the numerical runoff pdf shown in Figure 10 also includes fast components of the hydrologic response due to surface flow triggered by intense floods. In the case at hand, however, the fast component of the hydrologic response has characteristic times much shorter than 1 day [e.g., *Rinaldo et al.*, 2006b] and the runoff volume deriving from surface processes is relatively small, so that the surface contribution to the runoff pdf can be neglected (particularly at the daily timescale). The agreement between the numerical and the analytical runoff probability distributions is reasonably satisfactory, particularly if we consider the huge difference existing in the computational and operational burden required by the two models. Figure 10 therefore suggests that the analytical approach developed in this paper can be able to provide precious information on the probabilistic structure of daily runoff in river basins, at the minimum cost represented by the specification of a few macroparameters of clear physical

meaning. In particular, we stress the potential applicability of the approach developed to the prediction of seasonal runoff pdfs in ungauged basins, where all the model parameters shall be roughly estimated on the basis of a limited number of available data. From a gross geometrical descriptions of a catchment, in fact, one should easily argue reasonable estimates of the mean residence time, $1/k$, and of the basin extent, A. In the same time, naive climatic and pluviometric information allows to estimate the average runoff frequency, λ, and the average daily rainfall depth, which concur to define the scale parameter of the runoff probability distribution, γ_P.

[36] Therefore the tools developed seem to be significant in different contexts, in particular for large scale soil-atmosphere interactions and for the analysis of drought frequencies, which can be directly linked to the crossing properties of the randomly fluctuating discharge, $Q(t)$.

5. Conclusions

[37] The following conclusions are worth emphasizing.

[38] 1. The probability distribution of the slow component of the hydrologic response (i.e., the base flow) and its moment generating function have been derived by coupling a stochastic description of the soil moisture dynamics in river basins with a simplified transport model for subsurface flow.

[39] 2. Analytical solutions are achieved in two different cases, when the infiltration rates are upwardly bounded by episodical soil saturations and when the infiltration is unbounded. In both cases, the ensuing probability density function of base flows can be described by a Gamma distribution, whose shape is chiefly controlled by the ratio between the runoff frequency and the inverse of the mean residence time of subsurface flow.

[40] 3. The framework developed allows to link the probabilistic structure of base flows with simple (pluviometric, soil, vegetation and geomorphologic) macroparameters of clear physical meaning, with relevant implications for the ecohydrology of fluvial systems.

[41] 4. The comparison with numerical results, derived from the Monte Carlo application of a continuous, geomorphically based, rainfall-runoff model coupled with a stochastic climate generator to a real catchment located in northeastern Italy, suggests the ability of the approach proposed to capture the main features of runoff probability distributions in heterogeneous catchments at daily timescales.

References

Bathurst, J. C., and K. R. Cooley (1996), Use ofthe SHE hydrological modelling system to investigate basin response to snowmelt at Reynolds Creek, Idaho, *J. Hydrol.*, *175*, 181–211.

Bathurst, J. C., J. M. Wicks, and P. E. O'Connell (1995), The SHE/SHESED basin scale water flow and sediment transport modelling system, in *Computer Models of Watershed Hydrology*, pp. 563–594, Water Resour. Publ., Highlands Ranch, Colo.

Beven, K. J. (2001), *Rainfall-Runoff Modelling: The Primer*, John Wiley, Hoboken, N. J.

Beven, K. J., and M. J. Kirkby (1979), A physically based, variable contributing area model of basin hydrology, *Hydrol. Sci. Bull.*, *24*(1), 43–69.

Beven, K. J., R. Lamb, P. Quinn, R. Romanowicz, and J. Freer (1995), TOPMODEL, in *Computer Models of Watershed Hydrology*, pp. 627–668, Water Resour. Publ., Highlands Ranch, Colo.

Botter, G., and A. Rinaldo (2003), Scale effects on geomorphologic and kinematic dispersion, *Water Resour. Res.*, *39*(10), 1286, doi:10.1029/2003WR002154.

Botter, G., T. Settin, M. Marani, and A. Rinaldo (2006), A stochastic model of nitrate transport and cycling at basin scale, *Water Resour. Res.*, *42*, W04415, doi:10.1029/2005WR004599.

Boyd, M. J. (1978), A storage routing model relating drainage basin hydrology and geomorphology, *Water Resour. Res.*, *14*, 921–928.

Dagan, G. (1989), *Flow and Transport in Porous Formations*, Springer, New York.

Dingman, S. L. M. (1994), *Physical Hydrology*, MacMillan, New York.

Gupta, V. K., E. Waymire, and C. T. Wang (1980), A representation of an IUH from geomorphology, *Water Resour. Res.*, *16*, 862–885.

Kavetsky, D., G. Kuczera, and S. W. Frank (2003), Semidistributed hydrological modeling: A "saturation path" perspective on TOPMODEL and VIC, *Water Resour. Res.*, *39*(9), 1246, doi:10.1029/2003WR002122.

Laio, F. (2006), A vertically extended stochastic model of soil moisture in the root zone, *Water Resour. Res.*, *42*(2), W02406, doi:10.1029/2005WR004502.

Laio, F., A. Porporato, L. Ridolfi, and I. Rodriguez-Iturbe (2001), Plants in water-controlled ecosystems: Active role in hydrologic processes and response to water stress. II. Probabilistic soil moisture dynamics, *Adv. Water Resour.*, *24*, 707–723.

McGuire, K. J., J. J. McDonnel, M. Weiler, C. Kendall, B. L. McGlynn, J. M. Welker, and J. Seibert (2005), The role of topography on catchment scale water residence time, *Water Resour. Res.*, *41*, W05002, doi:10.1029/2004WR003657.

Milly, P. C. D., and K. A. Dunne (1993), Global water cycle to the water holding capacity of land, *J. Clim.*, *7*, 506–526.

Porporato, A., F. Laio, L. Ridolfi, and I. Rodriguez-Iturbe (2001), Plants in water controlled ecosystems: Active role in hydrological processes and response to water stress. III. Vegetation water stress, *Adv. Water Resour.*, *24*, 725–744.

Porporato, A., E. Daly, and I. Rodriguez-Iturbe (2004), Soil water balance and ecosystem response to climate change, *Am. Nat.*, *164*(5), 625–632.

Rinaldo, A., R. Rigon, and A. Marani (1991), Geomorphologic dispersion, *Water Resour. Res.*, *27*, 513–525.

Rinaldo, A., W. E. Dietrich, R. Rigon, G. K. Vogel, and I. Rodriguez-Iturbe (1995), Can one gauge the shape of a basin?, *Water Resour. Res.*, *31*, 1119–1127.

Rinaldo, A., E. Bertuzzo, and G. Botter (2005), Nonpoint source transport models from empiricism to coherent theoretical frameworks, *Ecol. Model.*, *184*, 19–35.

Rinaldo, A., G. Botter, E. Bertuzzo, A. Uccelli, T. Settin, and M. Marani (2006a), Transport at basin scales: 1. Theoretical framework, *Hydrol. Earth Syst. Sci.*, *10*, 19–30.

Rinaldo, A., G. Botter, E. Bertuzzo, A. Uccelli, T. Settin, and M. Marani (2006b), Transport at basin scales: 2. Applications, *Hydrol. Earth Syst. Sci.*, *10*, 31–48.

Robinson, J. S., M. Sivapalan, and J. D. Snell (1995), On the relative roles of hillslopes processes, channel routing and network geomorphology in the hydrologic response of natural catchments, *Water Resour. Res.*, *31*(12), 3089–3101.

Rodriguez-Iturbe, I., and A. Porporato (2004), *Ecohydrology of Water Controlled Ecosystems: Soil Moisture and Plant Dynamics*, Cambridge Univ. Press, New York.

Rodriguez-Iturbe, I., and A. Rinaldo (1997), *Fractal River Basins: Chance and Self-Organization*, Cambridge Univ. Press, New York.

Rodriguez-Iturbe, I., and J. B. Valdes (1979), The geomorphologic structure of hydrologic response, *Water Resour. Res.*, *15*, 1409–1420.

Rodriguez-Iturbe, I., D. R. Cox, and V. Isham (1987), Some models for rainfall based on stochastic point processes, *Proc. R. Soc. London, Ser. A*, *410*, 269–288.

Rodriguez-Iturbe, I., D. R. Cox, and V. Isham (1988), A point process model for rainfall: Further developments, *Proc. R. Soc. London, Ser. A*, *417*, 283–298.

Rodriguez-Iturbe, I., A. Porporato, L. Ridolfi, V. Isham, and D. Cox (1999), Probabilistic modelling of water balance at a point: The role of climate soil and vegetation, *Proc. R. Soc. London, Ser. A*, *455*, 3789–3805.

Rodriguez-Iturbe, I., V. Isham, D. Cox, S. Manfreda, and A. Porporato (2006), Space-time modelling of soil moisture: Stochastic rainfall forcing with heterogeneous vegetation, *Water Resour. Res.*, *42*, W06D05, doi:10.1029/2005WR004497.

Sivapalan, M., E. F. Wood, and K. J. Beven (1990), On hydrologic similarity: 3. A dimensionless flood frequency distribution, *Water Resour. Res.*, *26*, 43–58.

Troch, P. A., A. H. van Loon, and A. G. J. Hilberts (2004), Analytical solution of the linearized hillslope-storage Boussinesq equation for exponential hillslope width functions, *Water Resour. Res.*, *40*, W08601, doi:10.1029/2003WR002850.

Wetzel, P., and J.-T. Chang (1987), Concerning the relationship between evapotranspiration and soil moisture, *J. Clim. Appl. Meteorol.*, *26*, 18–27.

Wood, E. F., D. Lettenmaier, X. Liang, B. Nijssen, and S. W. Wetzel (1997), Hydrological modeling of continental-scale basins, *Annu. Rev. Earth Planet. Sci.*, *25*, 279–290.

————————————

G. Botter and A. Rinaldo, Dipartimento di Ingegneria Idraulica, Marittima e Geotecnica, Università di Padova, via Loredan 20, I-35131 Padova, Italy. (botter@idra.unipd.it)

A. Porporato, Department of Civil and Environmental Engineering, Duke University, Durham, NC 27708-0287, USA.

I. Rodriguez-Iturbe, Department of Civil and Environmental Engineering, Princeton University, Princeton, NJ 08544, USA.